Video Prediction Models as Rewards
for Reinforcement Learning

Alejandro Escontrela[†][*]   **Ademi Adeniji**[†]   **Wilson Yan**[†]

Ajay Jain   **Xue Bin Peng**   **Ken Goldberg**

Youngwoon Lee   **Danijar Hafner**   **Pieter Abbeel**

University of California, Berkeley

[†]Equal contribution

Abstract

Specifying reward signals that allow agents to learn complex behaviors is a long-standing challenge in reinforcement learning. A promising approach is to extract preferences for behaviors from unlabeled videos, which are widely available on the internet. We present Video Prediction Rewards (VIPER), an algorithm that leverages pretrained video prediction models as action-free reward signals for reinforcement learning. Specifically, we first train an autoregressive transformer on expert videos and then use the video prediction likelihoods as reward signals for a reinforcement learning agent. VIPER enables expert-level control without programmatic task rewards across a wide range of DMC, Atari, and RLBench tasks. Moreover, generalization of the video prediction model allows us to derive rewards for an out-of-distribution environment where no expert data is available, enabling cross-embodiment generalization for tabletop manipulation. We see our work as starting point for scalable reward specification from unlabeled videos that will benefit from the rapid advances in generative modeling. Source code and datasets are available on the project website: https://escontrela.me/viper

1   Introduction

Manually designing a reward function is laborious and often leads to undesirable outcomes [32]. This is a major bottleneck for developing general decision making agents with reinforcement learning (RL). A more scalable approach is to learn complex behaviors from *videos*, which can be easily acquired at scale for many applications (e.g., Youtube videos).

Previous approaches that learn behaviors from videos reward the similarity between the agent's current observation and the expert data distribution [37, 38, 30, 43]. Since their rewards only condition on the current observation, they cannot capture temporally meaningful behaviors. Moreover, the approaches with adversarial training schemes [30, 43] often result in mode collapse, which hinders generalization.
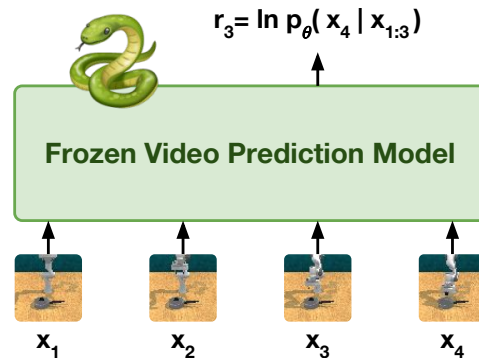

Figure 1: VIPER uses the next-token likelihoods of a frozen video prediction model as a general reward function for various tasks.

[*]Corresponding author: escontrela@berkeley.edu

(a) DeepMind Control Suite   (b) Robot Learning Benchmark   (c) Atari
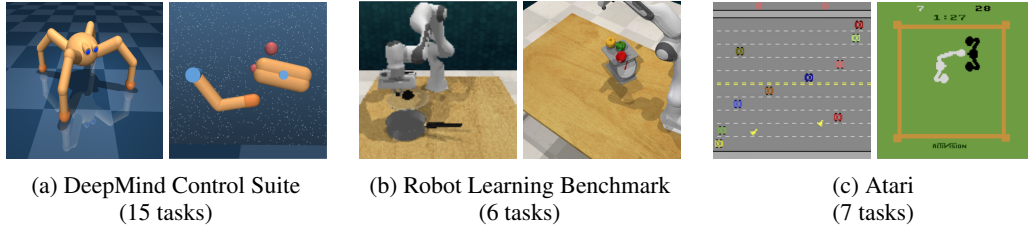(15 tasks)   (6 tasks)   (7 tasks)

Figure 2: VIPER achieves expert-level control directly from pixels without access to ground truth rewards or expert actions on 28 reinforcement learning benchmark tasks.

Other works fill in actions for the (action-free) videos using an inverse dynamics model [42, 8]. Dai et al. [8] leverage recent advances in generative modeling to capture multi-modal and temporally-coherent behaviors from large-scale video data. However, this multi-stage approach requires performing expensive video model rollouts to then label actions with a learned inverse dynamics model.

In this paper, we propose using Video Prediction Rewards (VIPER) for reinforcement learning. VIPER first learns a video prediction model from expert videos. We then train an agent using reinforcement learning to maximize the log-likelihood of agent trajectories estimated by the video prediction model, as illustrated in Figure 1. Directly leveraging the video model's likelihoods as a reward signal encourages the agent to match the video model's trajectory distribution. Additionally, rewards specified by video models inherently measure the temporal consistency of behavior, unlike observation-level rewards. Further, evaluating likelihoods is significantly faster than performing video model rollouts, enabling faster training times and more interactions with the environment.

We summarize the three key contributions of this paper as follows:

- We present VIPER: a novel, scalable reward specification algorithm which leverages rapid improvements in generative modeling to provide RL agents with rewards from unlabeled videos.
- We perform an extensive evaluation, and show that VIPER can achieve expert-level control **without task rewards** on 15 DMC tasks [44], 6 RLBench tasks [20], and 7 Atari tasks [3] (see examples in Figure 2 and Appendix A.5).
- We demonstrate that VIPER generalizes to different environments for which no training data was provided, enabling cross-embodiment generalization for tabletop manipulation.

Along the way, we discuss important implementation details that improve the robustness of VIPER.

2 Related Work

Learning from observations is an active research area which has led to many advances in imitation learning and inverse reinforcement learning [27, 1, 49]. This line of research is motivated by the fact that learning policies from expert videos is a scalable way of learning a wide variety of complex tasks, which does not require access to ground truth rewards, expert actions, or interaction with the expert. Scalable solutions to this problem would enable learning policies using the vast quantity of videos on the internet. Enabling policy learning from expert videos can be largely categorized into two approaches: (1) Behavioral cloning [31] on expert videos labelled with predicted actions and (2) reinforcement learning with a reward function learned from expert videos.

Labelling videos with predicted actions   An intuitive way of leveraging action-free expert videos is to guess which action leads to each transition in expert videos, then to mimic the predicted actions. Labelling videos with actions can be done using an inverse dynamics model, $p(a|s, s')$, which models an action distribution given the current and next observations. An inverse dynamics model can be learned from environment interactions [28, 42, 29] or a curated action-labelled dataset [2, 34]. Offline reinforcement learning [24] can be also used instead of behavioral cloning for more efficient use of video data with predicted actions [34]. However, the performance of this approach heavily depends on the quality of action labels predicted by an inverse dynamics model and the quantity and diversity of training data.

Reinforcement learning with videos Leveraging data from online interaction can further improve policies trained using unlabelled video data. To guide policy learning, many approaches have learned a reward function from videos by estimating the progress of tasks [37, 38, 25, 23] or the divergence between expert and agent trajectories [43, 30]. Adversarial imitation learning approaches [43, 30] learn a discriminator that discriminates transitions from the expert data and the rollouts of the current policy. Training a policy to maximize the discriminator error leads to similar expert and policy behaviors. However, the discriminator is prone to mode collapse, as it often finds spurious associations between task-irrelevant features and expert/agent labels [50, 19], which requires a variety of techniques to stabilize the adversarial training process [7]. In contrast, VIPER directly models the expert video distribution using recent generative modeling techniques [10, 47], which offers stable training and strong generalization.

Using video models as policies Recently, UniPi [8] uses advances in text-conditioned video generation models [33] to plan a trajectory. Once the future video trajectory is generated, UniPi executes the plan by inferring low-level controls using a learned inverse dynamics model. Instead of using slow video generations for planning, VIPER uses video prediction likelihoods to guide online learning of a policy.

3 Video Prediction Rewards

In this section, we propose Video Prediction Rewards (VIPER), which learns complex behaviors by leveraging the log-likelihoods of pre-trained video prediction models for reward specification. Our method does not require any ground truth rewards or action annotations, and only requires videos of desired agent behaviors. VIPER implements rewards as part of the environment, and can be paired with any RL algorithm. We overview the key components of our method below.

Algorithm 1: VIPER

Train video prediction model p_θ on expert videos.
while *not converged* **do**
 Choose action: $a_t \sim \pi(x_t)$
 Step environment: $x_{t+1} \leftarrow \text{env}(a_t)$
 Fill in reward: $r_t \leftarrow \ln p_\theta(x_{t+1} \mid x_{t-k:t}) + \beta r_t^{\text{expl}}$
 Add transition (x_t, a_t, r_t, x_{t+1}) to replay buffer.
 Train π from replay buffer using any RL algorithm.

3.1 Video Modeling

Likelihood-based video models are a popular paradigm of generative models trained to model the data distribution by maximizing an exact or lower bound on the log-likelihood of the data. These models have demonstrated their ability to fit highly multi-modal distributions and produce samples depicting complex dynamics, motion, and behaviors [40, 18, 17, 45].

Our method can integrate any video model that supports computing likelihoods over the joint distribution factorized in the following form:

$$\log p(x_{1:T}) = \sum_{t=1}^{T} \log p(x_t \mid x_{1:t-1}), \tag{1}$$

where $x_{1:T}$ is the full video consisting of T frames, $x_1, \ldots, x_T$. When using video models with limited context length k, it is common to approximate likelihoods of an entire video sequence with its subsequences of length k as follows:

$$\log p(x_{1:T}) \approx \sum_{t=1}^{T} \log p(x_t \mid x_{\max(1,t-k):t-1}). \tag{2}$$

In this paper, we use an autoregressive transformer model based on VideoGPT [47, 36] as our video generation model. We first train a VQ-GAN [10] to encode individual frames x_t into discrete codes z_t. Next, we learn an autoregressive transformer to model the distribution of codes z through the following maximum likelihood objective:

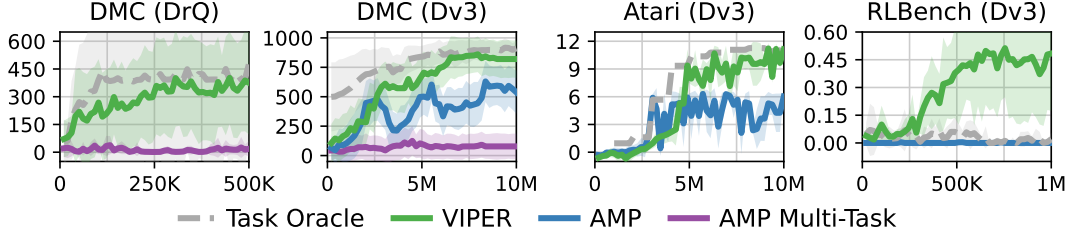$$\max_{\theta} \sum_{t=1}^{T} \sum_{i=1}^{Z} \log p_\theta(z_t^i \mid z_t^{1:i-1}, z_{1:t-1}), \tag{3}$$

3

Figure 3: Aggregate results across 15 DMC tasks, 7 Atari games, and 6 RLBench tasks. DMC results are provided for DrQ and DreamerV3 (Dv3) RL agents. Atari and RLBench results are reported for DreamerV3. Atari scores are computed using Human-Normalized Mean.

where z_t^i is the i-th code of the t-th frame, and Z is the total number of codes per frame. Computing the exact conditional likelihoods $p_\theta(x_t \mid x_{1:t-1})$ is intractable, as it requires marginalizing over all possible combinations of codes. Instead, we use the conditional likelihoods over the latent codes $p_\theta(z_t \mid z_{1:t-1})$ as an approximation. In our experiments, we show that these likelihoods are sufficient to capture the underlying dynamics of the videos.

Note that our choice of video model does not preclude the use of other video generation models, such as MaskGIT-based models [48, 45, 13] or diffusion models [18, 40]. However, we opted for an autoregressive model due to the favorable properties of being able to model complex distributions while retaining fast likelihood computation. Video model comparisons are performed in Section 4.4.

3.2 Reward Formulation

Given a pretrained video model, VIPER proposes an intuitive reward that maximizes the conditional log-likelihoods for each transition (x_t, a_t, x_{t+1}) observed by the agent:

$$r_t^{\text{VIPER}} \doteq \ln p_\theta(x_{t+1} \mid x_{1:t}). \tag{4}$$

This reward incentivizes the agent to find the most likely trajectory under the expert video distribution as modeled by the video model. However, the most probable sequence does not necessarily capture the distribution of behaviors we want the agent to learn.

For example, when flipping a weighted coin with $p(\text{heads} = 0.6)$ 1000 times, *typical sequences* will count roughly 600 heads and 400 tails, in contrast to the most probable sequence of 1000 heads that will basically never be seen in practice [39]. Similarly, the most likely image under a density model trained on MNIST images is often the image of only background without a digit, despite this never occurring in the dataset [26]. In the reinforcement learning setting, an additional issue is that solely optimizing a dense reward such as r_t^{VIPER} can lead to early convergence to local optima.

To overcome these challenges, we take the more principled approach of matching the agent's trajectory distribution $q(x_{1:T})$ to the sequence distribution $p_\theta(x_{1:T})$ of the video model by minimizing the KL-divergence between the two distributions [41, 15]:

$$\text{KL}\big[q(x_{1:T}) \,\big\|\, p(x_{1:T})\big] = \underbrace{\text{E}_q\big[-\ln p_\theta(x_{1:T})\big]}_{\text{cross-entropy}} - \underbrace{\text{H}\big[q(x_{1:T})\big]}_{\text{entropy}}$$

$$= -\sum_{t=1}^{T}\left[\text{E}_q\big[\underbrace{\ln p_\theta(x_{t+1} \mid x_{1:t})}_{r_t^{\text{VIPER}}}\big] + \underbrace{\text{H}\big[q(x_{t+1} \mid x_{1:t})\big]}_{\text{exploration term}}\right], \tag{5}$$

The KL objective shows that for the agent to match the video distribution under the video prediction model, it has to not only maximize the VIPER reward but also balance this reward while maintaining high entropy over its input sequences [21]. In the reinforcement learning literature, the entropy bonus over input trajectories corresponds to an exploration term that encourages the agent to explore and inhabit a diverse distribution of sequences within the regions of high probability under the video prediction model. This results in the final reward function that the agent maximizes:

$$r_t^{\text{KL}} \doteq r_t^{\text{VIPER}} + \beta\, r_t^{\text{expl}}, \tag{6}$$

where β determines the amount of exploration. To efficiently compute the likelihood reward, we approximate the context frames with a sliding window as discussed in Equation 2:

$$r_t^{\text{VIPER}} \approx \ln p_\theta(x_{t+1} \mid x_{\max(1,t-k):t}). \tag{7}$$

4

Figure 1 shows the process of computing rewards using log probabilities under the video prediction model. VIPER is agnostic to the choice of exploration reward and in this paper we opt for Plan2Explore [35] and RND [5].

3.3 Data Curation

In this work, we explore whether VIPER provides adequate reward signal for learning low-level control. We utilize the video model likelihoods provided by an autoregressive video prediction model pre-trained on data from a wide variety of environments. We curate data by collecting expert video trajectories from task oracles and motion planning algorithms with access to state information. Fine-tuning large text-conditioned video models [33, 45, 40] on expert videos would likely lead to improved generalization performance beyond the curated dataset, and would make for an interesting future research direction. We explore the favorable generalization capabilities of video models trained on small datasets, and explore how this leads to more general reward functions in Section 4.3.

4   Experiments

We evaluate VIPER on 28 different tasks across the three domains shown in Figure 2. We utilize 15 tasks from the DeepMind Control (DMC) suite [44], 7 tasks from the Atari Gym suite [4], and 6 tasks from the Robot Learning Benchmark (RLBench) [20]. We compare VIPER agents to variants of Adversarial Motion Priors (AMP) [30], which uses adversarial training to learn behaviors from reward-free and action-free expert data. All agents are trained using raw pixel observations from the environment, with no access to state information or task rewards. In our experiments, we aim to answer the following questions:

1. Does VIPER provide an adequate learning signal for solving a variety of tasks? (Section 4.2)
2. Do video models trained on many different tasks still provide useful rewards? (Section 4.2)
3. Can the rewards generalize to novel scenarios where no expert data is available? (Section 4.3)
4. What implementation details matter when using video model likelihoods as rewards? (Section 4.4)

4.1   Video Model Training Details

Training data   To collect expert videos in DMC and Atari tasks, **Task Oracle** RL agents are trained until convergence with access to ground truth state information and task rewards. After training, videos of the top k episodes out of 1000 episode rollouts for each task are sampled as expert videos, where $k = 50$ and 100 for DMC and Atari, respectively. For RLBench, a sampling-based motion planning algorithm with access to full state information is used to gather 100 demos for each task, where selected tasks range from "easy" to "medium".

Video model training   We train a *single* autoregressive video model for each suite of tasks. Example images for each suite are shown in Appendix A.5. For DMC, we train a single VQ-GAN across all tasks that encodes 64×64 images to 8×8 discrete codes. Similarly for RLBench and Atari, we train VQ-GANs across all tasks within each domain, but encode 64×64 images to 16×16 discrete codes. In practice, the level of VQ compression depends on the visual complexity of the environment – more texturally simple environments (e.g., DMC) allow for higher levels of spatial compression. We follow the original VQ-GAN architecture [10], consisting of a CNN encoder and decoder. We train VQ-GAN with a batch size of 128 and learning rate 10^{-4} for 200k iterations.
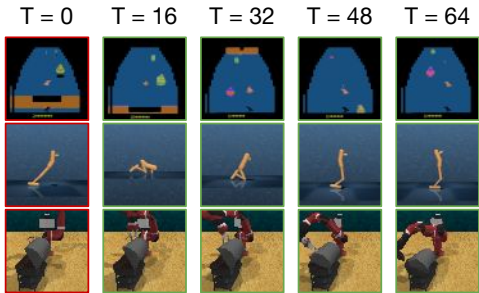

Figure 4: Video model rollouts for 3 different evaluation environments.

To train our video models, we encode each frame of the trajectory and stack the codes temporally to form an encoded 3D video tensor. Similar to VideoGPT [47], the encoded VQ codes for all video frames are jointly modeled using an autoregressive transformer in raster scan order. For DMC and Atari, we train on 16 frames at a time with a one-hot label for task conditioning. For RLBench,

we train both single-task and multi-task video models on 4 frames with frame skip 4. We add the one-hot task label for the multi-task model used in our cross-embodiment generalization experiments in Section 4.3. We perform task conditioning identical to the class conditioning mechanism in VideoGPT, with learned gains and biases specific to each task ID for each normalization layer.

Figure 4 shows example video model rollouts for each domain. In general, our video models are able to accurately capture the dynamics of each environment to produce probable futures. Further details on model architecture and hyperparameters can be found in Appendix A.2. All models are trained on TPUv3-8 instances which are approximately similar to 4 Nvidia V100 GPUs.

4.2 Video Model Likelihoods as Rewards for Reinforcement Learning

To learn behaviors from expert videos, we provide reward signals using Equation 6 in VIPER and the discriminator error in AMP. Both VIPER and AMP are agnostic to the choice of RL algorithm; but, in this paper, we evaluate our approach and baselines with two popular RL algorithms: DrQ [22] and DreamerV3 [16]. We use Random Network Distillation [5] (model-free) as the exploration objective for DrQ, and Plan2Explore [35] (model-based) for DreamerV3. Hyperparameters for each choice of RL algorithm are shown in Appendix A.3. We compare VIPER to two variants of the AMP algorithm: the single-task variant where only expert videos for the specific task are provided to the agent, and the multi-task case where expert videos for all tasks are provided to the agent.

As outlined in Algorithm 1, we compute Equation 6 for every environment step to label the transition with a reward before adding it to the replay buffer for policy optimization. In practice, batching Equation 6 across multiple environments and leveraging parallel likelihood evaluation leads to only a small decrease in training speed. DMC agents were trained using 1 Nvidia V100 GPU, while Atari and RLBench agents were trained using 1 Nvidia A100 GPU.
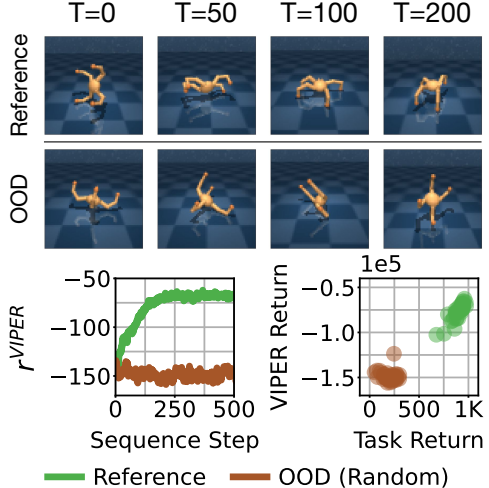

Figure 5: VIPER incentivizes the agent to maximize trajectory likelihood under the video model. As such, it provides high rewards for reference (expert) sequences, and low rewards for unlikely behaviors. Mean rewards r^{VIPER} and returns are computed across 40 trajectories.

We first verify whether VIPER provides meaningful rewards aligned with the ground truth task rewards. Figure 5 visualizes the ground truth task rewards and our log-likelihood rewards (Equation 7) for a reference (expert) trajectory and a random out-of-distribution trajectory. In the reward curves on the left, VIPER starts to predict high rewards for the expert transitions once the transitions becomes distinguishable from a random trajectory, while it consistently outputs low rewards for out-of-distribution transitions. The return plot on the right clearly shows positive correlation between returns of the ground truth reward and our proposed reward.

Then, we measure the task rewards when training RL agents with predicted rewards from VIPER and baselines and report the aggregated results for each suite and algorithm in Figure 3. The full results can be found in Appendix A.4.

In DMC, VIPER achieves near expert-level performance from pixels with our video prediction rewards alone. Although VIPER slightly underperforms Task Oracle, this is surprising as the Task Oracle uses *full state information* along with *dense task rewards*. VIPER outperforms both variants of AMP. Worth noting is the drastic performance difference between the single-task and multi-task AMP algorithms. This performance gap can possibly be attributed to mode collapse, whereby the discriminator classifies all frames for the current task as fake samples, leading to an uninformative reward signal for the agent. Likelihood-based video models, such as VIPER, are less susceptible to mode collapse than adversarial methods.

In Atari, VIPER approaches the performance of the Task Oracle trained with the original sparse task reward, and outperforms the AMP baseline. Shown in Figure 6, we found that masking the scoreboard in each Atari environment when training the video model improved downstream RL performance.
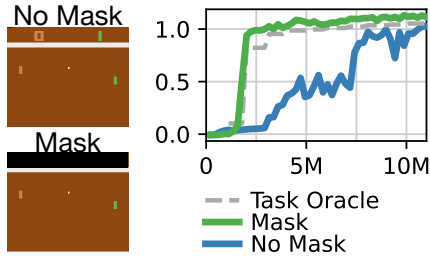
6

No Mask

Mask

Figure 6: RL training curves on Atari Pong when using VIPER trained with or without masking the scoreboard.

Since the video model learns to predict all aspects of the data distribution, including the scoreboard, it tends to provide noisier reward signal during policy training when the agent encounters out-of-distributions scores not seen by the video model. For example, expert demos for Pong only contain videos where the player scores and the opponent's score is always zero. During policy training, we observe that the Pong agent tends to exhibit more erratic behaviors as soon as the opponent scores at least one point, whereas when masking the scoreboard, learned policies are generally more stable. These results suggest the potential benefits of finetuning large video models on expert demos to learn more generalizable priors, as opposed to training from scratch.

For RLBench, VIPER outperforms the Task Oracle because RLBench tasks provide very sparse rewards after long sequences of actions, which pose a challenging objective for RL agents. VIPER instead provides a dense reward extracted from the expert videos, which helps learn these challenging tasks. When training the video model, we found it beneficial to train at a reduced frame rate, accomplished by subsampling video sequences by a factor of 4. Otherwise, we observed the video model would assign high likelihoods to stationary trajectories, resulting in learned policies rarely moving and interacting with the scene. We hypothesize that this may be partially due to the high control frequency of the environment, along with the initial slow acceleration of the robot arm in demonstrations, resulting in very little movement between adjacent frames. When calculating likelihoods for reward computation, we similarly input observations strided by time, e.g., $p(x_t \mid x_{t-4}, x_{t-8}, \dots)$.

4.3 Generalization of Video Prediction Rewards

Prior works in the space of large, pretrained generative models have shown a powerful ability to generalize beyond the original training data, demonstrated by their ability to produce novel generations (e.g., unseen text captions for image or video generation [33, 45, 40]) as well as learn more generalizable models from limited finetuning data [8, 46]. Both capabilities provide promising directions for extending large video generation models to VIPER, where we can leverage text-video models to capture priors specified by text commands, or finetune on a small set of demonstrations to learn a task-specific prior that better generalizes to novel states.

In this section, we seek to understand how this generalization can be used to learn more general reward functions. We train a model on two datasets of different robot arms, and evaluate the *cross-embodiment generalization* capabilities of the model. Specifically, we gather demonstrations for 23
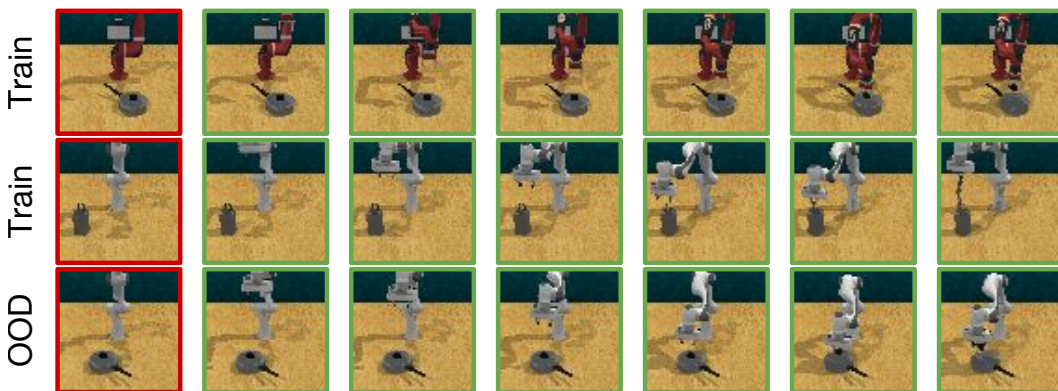

Figure 7: Sampled video predictions for in distribution reference videos (Train) and an OOD arm/task combination (OOD). The video model displays cross-embodiment generalization to arm/task combination not observed in the training data. Video model generalization can enable specifying new tasks where no reference data is available.
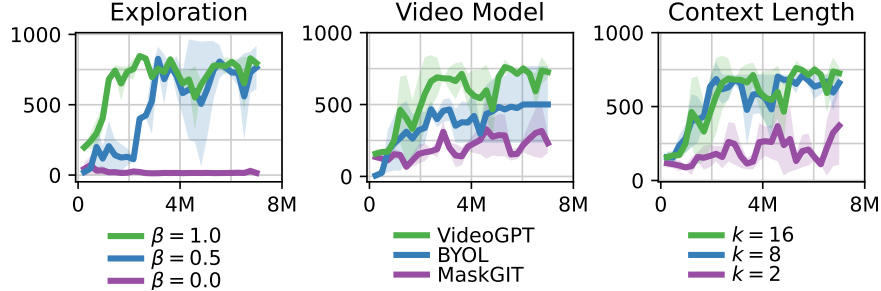
7

Figure 9: Effect of exploration reward term, video model choice, and context length on downstream RL performance. An equally weighted exploration reward term and longer video model context leads to improved performance. MaskGIT substantially underperforms VideoGPT as a choice of video model. The BYOL model performs moderately due to the deterministic architecture not properly handling multi-modality.

tasks on the Rethink Robotics Sawyer Arm, and demonstrations for 30 tasks on the Franka Panda robotic arm, where only 20 tasks are overlapping between arms. We then train a task-conditioned autoregressive video model on these demonstration videos and evaluate the video model by querying unseen arm/task combinations, where a single initial frame is used for open loop predictions.

Sample video model rollouts for in distribution training tasks and an OOD arm/task combination are shown in Figure 7. Even though the video model was not directly trained on demonstrations of the Franka Panda arm to solve the saucepan task in RLBench, it is able to generate reasonable trajectories for the arm and task combination. Figure 8 further validates this observation by assigning higher likelihood to expert videos (Ref) compared to random robot trajectories (Rand). We observe that these generaliza-
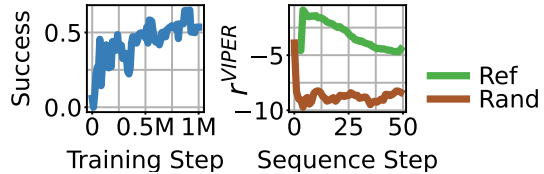

Figure 8: (Left) Training curve for RL agent trained with VIPER on OOD task. (Right) Task-conditional likelihood for reference and random trajectory for an OOD task.

tion capabilities also extend to downstream RL, where we use our trained video model with VIPER to learn a policy for the Franka Robot arm to solve an OOD task without requiring demos for that specific task and arm combination. These results demonstrate a promising direction for future work in applying VIPER to larger scale video models that will be able to better generalize and learn desired behaviors only through a few demonstrations.

4.4 Ablation Studies

In this section, we study the contributions of various design decisions when using video prediction models as rewards: (1) how to weight the exploration objective, (2) which video model to use, and (3) what context length to use. Ablation studies are performed across DMC tasks.

Exploration objective   As discussed in subsection 3.2, an exploration objective may help the RL agent learn a distribution of behaviors that closely matches the distribution of the original data and generalizes, while preventing locally optimal solutions. In Figure 9, we ablate the β parameter introduced in Equation 6 using a VideoGPT-like model as the VIPER backbone. $\beta = 0$ corresponds to no exploration objective, whereas $\beta = 1$ signifies equal weighting between r^{VIPER} and r^{expl}. We ablate the exploration objective using the Plan2Explore [35] reward, which provides the agent with a reward proportional to the disagreement between an ensemble of one-step dynamics models. Using no exploration objective causes the policy's behavior to collapse, while increasing the weight of the exploration objective leads to improved performance.

Video model   Although our experiments focus on using an autoregressive VideoGPT-like model to compute likelihoods, VIPER generally allows for any video model that supports computing conditional likelihoods or implicit densities.

8

Figure 9 shows additional ablations replacing our VideoGPT model with a similarly sized MaskGIT [6] model, where frames are modeled with MaskGIT over space, and autoregressive over time. MaskGIT performs substantially worse than the VideoGPT model, which is possibly due to noisier likelihoods from parallel likelihood computation. In addition, while VideoGPT only requires 1 forward pass to compute likelihood, MaskGIT requires as many as 8 forward passes on the sequence of tokens for a frame, resulting in an approximately $8\times$ slowdown in reward computation, and $2.5\times$ in overall RL training.

Finally, we evaluate the performance of a video model that computes implicit densities using a negative distance metric between online predictions and target encodings with a recurrent Bootstrap Your Own Latent (BYOL) architecture [12, 11]. We refer the reader to Appendix A.1 for more details about the implementation. While BYOL outperforms MaskGIT in Figure 9, its deterministic recurrent architecture is unable to predict accurate embeddings more than a few steps into the future. This limits the ability of the learned reward function to capture temporal dynamics. We observe that agents trained with BYOL often end up in a stationary pose, which achieves high reward from the BYOL model.

Context length The context length k of the video model is an important choice in determining how much history to incorporate into the conditional likelihood. At the limit where $k = 0$, the reward is the unconditional likelihood over each frame. Such a choice would lead to stationary behavior on many tasks. Figure 9 shows that increasing the context length can help improve performance when leveraging a VideoGPT-based model for downstream RL tasks, subject to diminishing returns. We hypothesize that a longer context length may help for long-horizon tasks.

5 Conclusion

This paper presents Video Prediction Rewards (VIPER), a general algorithm that enables agents to learn behaviors from videos of experts. To achieve this, we leverage a simple pre-trained autoregressive video model to provide rewards for a reinforcement learning agent. These rewards are parameterized as the conditional probabilities of a particular frame given a context past of frames. In addition, we include an entropy maximization objective to ensure that the agent learns diverse behaviors which match the video model's trajectory distribution. VIPER succeeds across 3 benchmarks and 28 tasks, including the DeepMind Control Suite, Atari, and the Reinforcement Learning Benchmark. We find that simple data augmentation techniques can dramatically improve the effectiveness of VIPER. We also show that VIPER generalizes to out-of-distribution tasks for which no demonstrations were provided. Moreover, VIPER can learn reward functions for a wide variety of tasks using a single video model, outperforming AMP [30], which suffers from mode collapse as the diversity of the expert videos increases.

Limitations of our work include that VIPER is trained using in-domain data of expert agents, which is not a readily-available data source in the real world. Additionally, video prediction rewards trained on stochastic data may lead the agent to prefer states that minimize the video model's uncertainty, which may lead to sub-optimal behaviors. This challenge may be present for cases where either the environment is stochastic or the demonstrator provides noisy demonstrations. Moreover, selecting the right trade-off between VQCode size and context length has a significant impact on the quality of the learned rewards, with small VQCodes failing to model important components of the environment (e.g., the ball in Atari Breakout) and short context lengths leading to myopic behaviors which results in poor performance. Exploring alternative video model architectures for VIPER would likely be a fruitful research direction.

To improve the generalization capabilities of VIPER, larger pre-trained video models are necessary. Future work will explore how fine-tuning or human preferences can be used to improve video prediction rewards. Using text-to-video models remain another interesting direction for future work in extracting text-conditioned task-specific priors from a pretrained video model. In addition, extending this line of work to leverage Video Diffusion Models [18] as video prediction rewards may lead to interesting outcomes.

Acknowledgments and Disclosure of Funding

References

[1] Pieter Abbeel and Andrew Y Ng. Apprenticeship learning via inverse reinforcement learning. In *International Conference on Machine Learning*, 2004.

[2] Bowen Baker, Ilge Akkaya, Peter Zhokhov, Joost Huizinga, Jie Tang, Adrien Ecoffet, Brandon Houghton, Raul Sampedro, and Jeff Clune. Video pretraining (vpt): Learning to act by watching unlabeled online videos. In *Advances in Neural Information Processing Systems*, 2022.

[3] Marc G Bellemare, Yavar Naddaf, Joel Veness, and Michael Bowling. The arcade learning environment: An evaluation platform for general agents. *Journal of Artificial Intelligence Research*, 47:253–279, 2013.

[4] Greg Brockman, Vicki Cheung, Ludwig Pettersson, Jonas Schneider, John Schulman, Jie Tang, and Wojciech Zaremba. Openai gym. *arXiv preprint arXiv:1606.01540*, 2016.

[5] Yuri Burda, Harrison Edwards, Amos Storkey, and Oleg Klimov. Exploration by random network distillation. In *International Conference on Learning Representations*, 2019.

[6] Huiwen Chang, Han Zhang, Lu Jiang, Ce Liu, and William T Freeman. Maskgit: Masked generative image transformer. In *Proceedings of the IEEE/CVF Conference on Computer Vision and Pattern Recognition*, pages 11315–11325, 2022.

[7] Soumith Chintala, Emily Denton, Martin Arjovsky, and Michael Mathieu. How to train a gan? tips and tricks to make gans work. https://github.com/soumith/ganhacks, 2020.

[8] Yilun Dai, Mengjiao Yang, Bo Dai, Hanjun Dai, Ofir Nachum, Josh Tenenbaum, Dale Schuurmans, and Pieter Abbeel. Learning universal policies via text-guided video generation. *arXiv preprint arXiv:2302.00111*, 2023.

[9] Andreas Doerr, Christian Daniel, Martin Schiegg, Nguyen-Tuong Duy, Stefan Schaal, Marc Toussaint, and Trimpe Sebastian. Probabilistic recurrent state-space models. In *International conference on machine learning*, pages 1280–1289. PMLR, 2018.

[10] Patrick Esser, Robin Rombach, and Bjorn Ommer. Taming transformers for high-resolution image synthesis. In *Proceedings of the IEEE/CVF conference on computer vision and pattern recognition*, pages 12873–12883, 2021.

[11] Jean-Bastien Grill, Florian Strub, Florent Altché, Corentin Tallec, Pierre Richemond, Elena Buchatskaya, Carl Doersch, Bernardo Avila Pires, Zhaohan Guo, Mohammad Gheshlaghi Azar, et al. Bootstrap your own latent-a new approach to self-supervised learning. In *Advances in neural information processing systems*, volume 33, pages 21271–21284, 2020.

[12] Zhaohan Guo, Shantanu Thakoor, Miruna Pîslar, Bernardo Avila Pires, Florent Altché, Corentin Tallec, Alaa Saade, Daniele Calandriello, Jean-Bastien Grill, Yunhao Tang, et al. Byol-explore: Exploration by bootstrapped prediction. In *Advances in neural information processing systems*, volume 35, pages 31855–31870, 2022.

[13] Agrim Gupta, Stephen Tian, Yunzhi Zhang, Jiajun Wu, Roberto Martín-Martín, and Li Fei-Fei. Maskvit: Masked visual pre-training for video prediction. *arXiv preprint arXiv:2206.11894*, 2022.

[14] Danijar Hafner, Timothy Lillicrap, Ian Fischer, Ruben Villegas, David Ha, Honglak Lee, and James Davidson. Learning latent dynamics for planning from pixels. In *International conference on machine learning*, pages 2555–2565. PMLR, 2019.

[15] Danijar Hafner, Pedro A Ortega, Jimmy Ba, Thomas Parr, Karl Friston, and Nicolas Heess. Action and perception as divergence minimization. *arXiv preprint arXiv:2009.01791*, 2020.

[16] Danijar Hafner, Jurgis Pasukonis, Jimmy Ba, and Timothy Lillicrap. Mastering diverse domains through world models. *arXiv preprint arXiv:2301.04104*, 2023.

[17] Jonathan Ho, William Chan, Chitwan Saharia, Jay Whang, Ruiqi Gao, Alexey Gritsenko, Diederik P Kingma, Ben Poole, Mohammad Norouzi, David J Fleet, et al. Imagen video: High definition video generation with diffusion models. *arXiv preprint arXiv:2210.02303*, 2022.

[18] Jonathan Ho, Tim Salimans, Alexey Gritsenko, William Chan, Mohammad Norouzi, and David J Fleet. Video diffusion models. In *Advances in Neural Information Processing Systems*, 2022.

[19] Andrew Jaegle, Yury Sulsky, Arun Ahuja, Jake Bruce, Rob Fergus, and Greg Wayne. Imitation by predicting observations. In *International Conference on Machine Learning*, pages 4665–4676. PMLR, 2021.

[20] Stephen James, Zicong Ma, David Rovick Arrojo, and Andrew J. Davison. Rlbench: The robot learning benchmark & learning environment. *IEEE Robotics and Automation Letters*, 2020.

[21] Edwin T Jaynes. Information theory and statistical mechanics. *Physical review*, 106(4):620, 1957.

[22] Ilya Kostrikov, Denis Yarats, and Rob Fergus. Image augmentation is all you need: Regularizing deep reinforcement learning from pixels. In *International Conference on Learning Representations*, 2021.

[23] Youngwoon Lee, Andrew Szot, Shao-Hua Sun, and Joseph J. Lim. Generalizable imitation learning from observation via inferring goal proximity. In *Neural Information Processing Systems*, 2021.

[24] Sergey Levine, Aviral Kumar, George Tucker, and Justin Fu. Offline reinforcement learning: Tutorial, review, and perspectives on open problems. *arXiv preprint arXiv:2005.01643*, 2020.

[25] YuXuan Liu, Abhishek Gupta, Pieter Abbeel, and Sergey Levine. Imitation from observation: Learning to imitate behaviors from raw video via context translation. In *IEEE International Conference on Robotics and Automation*, 2018.

[26] Eric Nalisnick, Akihiro Matsukawa, Yee Whye Teh, Dilan Gorur, and Balaji Lakshminarayanan. Do deep generative models know what they don't know? In *International Conference on Learning Representations*, 2019.

[27] Andrew Y. Ng and Stuart J. Russell. Algorithms for inverse reinforcement learning. In *International Conference on Machine Learning*, 2000.

[28] Scott Niekum, Sarah Osentoski, George Konidaris, Sachin Chitta, Bhaskara Marthi, and Andrew G Barto. Learning grounded finite-state representations from unstructured demonstrations. *The International Journal of Robotics Research*, 34(2):131–157, 2015.

[29] Deepak Pathak, Parsa Mahmoudieh, Michael Luo, Pulkit Agrawal, Dian Chen, Fred Shentu, Evan Shelhamer, Jitendra Malik, Alexei A. Efros, and Trevor Darrell. Zero-shot visual imitation. In *International Conference on Learning Representations*, 2018.

[30] Xue Bin Peng, Ze Ma, Pieter Abbeel, Sergey Levine, and Angjoo Kanazawa. AMP: adversarial motion priors for stylized physics-based character control. *ACM Transactions on Graphics (TOG)*, 40(4):1–20, 2021.

[31] Dean A Pomerleau. Alvinn: An autonomous land vehicle in a neural network. In *Advances in Neural Information Processing Systems*, pages 305–313, 1989.

[32] Martin Riedmiller, Roland Hafner, Thomas Lampe, Michael Neunert, Jonas Degrave, Tom Wiele, Vlad Mnih, Nicolas Heess, and Jost Tobias Springenberg. Learning by playing solving sparse reward tasks from scratch. In *International conference on machine learning*, pages 4344–4353. PMLR, 2018.

[33] Chitwan Saharia, William Chan, Saurabh Saxena, Lala Li, Jay Whang, Emily Denton, Seyed Kamyar Seyed Ghasemipour, Burcu Karagol Ayan, S. Sara Mahdavi, Rapha Gontijo Lopes, Tim Salimans, Jonathan Ho, David J Fleet, and Mohammad Norouzi. Photorealistic text-to-image diffusion models with deep language understanding. In *Advances in Neural Information Processing Systems*, 2022.

[34] Karl Schmeckpeper, Oleh Rybkin, Kostas Daniilidis, Sergey Levine, and Chelsea Finn. Reinforcement learning with videos: Combining offline observations with interaction. In *Conference on Robot Learning*, 2021.

[35] Ramanan Sekar, Oleh Rybkin, Kostas Daniilidis, Pieter Abbeel, Danijar Hafner, and Deepak Pathak. Planning to explore via self-supervised world models. In *International Conference on Machine Learning*, 2020.

[36] Younggyo Seo, Kimin Lee, Fangchen Liu, Stephen James, and Pieter Abbeel. Harp: Autoregressive latent video prediction with high-fidelity image generator. In *2022 IEEE International Conference on Image Processing (ICIP)*, pages 3943–3947. IEEE, 2022.

[37] Pierre Sermanet, Kelvin Xu, and Sergey Levine. Unsupervised perceptual rewards for imitation learning. *Robotics: Science and Systems*, 2017.

[38] Pierre Sermanet, Corey Lynch, Yevgen Chebotar, Jasmine Hsu, Eric Jang, Stefan Schaal, and Sergey Levine. Time-contrastive networks: Self-supervised learning from video. In *IEEE International Conference on Robotics and Automation*, pages 1134–1141, 2018.

[39] Claude Elwood Shannon. A mathematical theory of communication. *ACM SIGMOBILE mobile computing and communications review*, 5(1):3–55, 2001.

[40] Uriel Singer, Adam Polyak, Thomas Hayes, Xi Yin, Jie An, Songyang Zhang, Qiyuan Hu, Harry Yang, Oron Ashual, Oran Gafni, Devi Parikh, Sonal Gupta, and Yaniv Taigman. Make-a-video: Text-to-video generation without text-video data. In *International Conference on Learning Representations*, 2023.

[41] Emanuel Todorov. Efficient computation of optimal actions. *Proceedings of the national academy of sciences*, 106(28):11478–11483, 2009.

[42] Faraz Torabi, Garrett Warnell, and Peter Stone. Behavioral cloning from observation. In *International Joint Conferences on Artificial Intelligence*, 2018.

[43] Faraz Torabi, Garrett Warnell, and Peter Stone. Generative adversarial imitation from observation. *arXiv preprint arXiv:1807.06158*, 2018.

[44] Saran Tunyasuvunakool, Alistair Muldal, Yotam Doron, Siqi Liu, Steven Bohez, Josh Merel, Tom Erez, Timothy Lillicrap, Nicolas Heess, and Yuval Tassa. dm_control: Software and tasks for continuous control. *Software Impacts*, 6:100022, 2020. ISSN 2665-9638.

[45] Ruben Villegas, Mohammad Babaeizadeh, Pieter-Jan Kindermans, Hernan Moraldo, Han Zhang, Mohammad Taghi Saffar, Santiago Castro, Julius Kunze, and Dumitru Erhan. Phenaki: Variable length video generation from open domain textual description. *arXiv preprint arXiv:2210.02399*, 2022.

[46] Jason Wei, Maarten Bosma, Vincent Zhao, Kelvin Guu, Adams Wei Yu, Brian Lester, Nan Du, Andrew M. Dai, and Quoc V Le. Finetuned language models are zero-shot learners. In *International Conference on Learning Representations*, 2022.

[47] Wilson Yan, Yunzhi Zhang, Pieter Abbeel, and Aravind Srinivas. Videogpt: Video generation using vq-vae and transformers. *arXiv preprint arXiv:2104.10157*, 2021.

[48] Lijun Yu, Yong Cheng, Kihyuk Sohn, José Lezama, Han Zhang, Huiwen Chang, Alexander G Hauptmann, Ming-Hsuan Yang, Yuan Hao, Irfan Essa, et al. Magvit: Masked generative video transformer. *arXiv preprint arXiv:2212.05199*, 2022.

[49] Brian D Ziebart, Andrew L Maas, J Andrew Bagnell, and Anind K Dey. Maximum entropy inverse reinforcement learning. In *Association for the Advancement of Artificial Intelligence*, 2008.

[50] Konrad Zolna, Scott Reed, Alexander Novikov, Sergio Gomez Colmenarej, David Budden, Serkan Cabi, Misha Denil, Nando de Freitas, and Ziyu Wang. Task-relevant adversarial imitation learning. In *Conference on Robot Learning*, 2020.

A Appendix

A.1 Bootstrap Your Own Latent Details

Model Architecture. The BYOL model used in this work derives from the recurrent BYOL-Explore architecture proposed in [12], with a few modifications. Namely Guo et al. propose BYOL-Explore, a multi-step predictive latent world model. The BYOL-Explore architecture trains an online network using targets generated by an exponential moving average target network on future observations. Observations o_t are first encoded into an observation representation $f_\theta(o_t)$. Online predictions are computed by then encoding the observation representation using a closed-loop RNN $h_\theta^c(f_\theta(o_t))$. Guo et al. also pass actions into the closed loop RNN, but we wish to learn an action-free reward mechanism that can be trained solely from videos. At each timestep, the carry b_t from the closed loop RNN is then fed into an open-loop RNN h_θ^o which predicts open-loop representations K steps into the future: $(b_{t,k} \in \mathcal{R}^{\mathcal{M}})_{k=1}^{K-1}$, where $b_{t,k} = h_\theta^o(b_{t,k-1})$. The original BYOL-Explore architecture feeds actions a_{t+k+1} as inputs to the open loop cell h_θ^o as well, but we opt to omit these inputs for the same reason outlined above.

Given the deterministic RNN architecture used to predict online targets, omitting the action conditioning may lead to poor performance in multi-modal or stochastic environments. A more principled approach would utilize a probabilistic recurrent state space model [9, 14] to account for the multi-modality of futue states. We leave this approach to future work.

Finally, a predictor head $g_\theta(b_{t,k})$ outputs online predictions. We refer the reader to [12] for a figure of the outlined architecture.

The target network is an observation encoder f_ϕ whose parameters are an exponential moving average of f_θ. The loss function for the online network is then defined as:

$$\mathcal{L}_{\text{BYOL-Explore}}(\theta, t, k) = \left\| \frac{g_\theta(b_{t,k})}{\|g_\theta(b_{t,k})\|_2} - \text{sg}\left(\frac{f_\phi(o_{t+k})}{\|f_\phi(o_{t+k})\|_2} \right) \right\|_2^2,$$

$$\mathcal{L}_{\text{BYOL-Explore}}(\theta) = \frac{1}{B(T-1)} \sum_{t=0}^{T-2} \frac{1}{K(t)} \sum_{k=1}^{K(t)} \mathcal{L}_{\text{BYOL-Explore}}(\theta, t, k),$$

where $K(t) = \min(K, T-1-t)$ is the valid open-loop horizon for a trajectory of length T and sg is the stop-gradient operator.

Computing Rewards. The uncertainty associated with the transition (o_t, a_t, o_{t+1}) is the sum of the corresponding prediction losses:

$$\ell_t = \sum_{p+q=t+1} \mathcal{L}_{\text{BYOL-Explore}}(\theta, j, p, q),$$

where $0 \le p \le T-2$, $1 \le q \le K$ and $0 \le t \le T-2$. This accumulates all the losses corresponding to the latent dynamics model uncertainties relative to the observation o_{t+1}. For our purposes, we calculate rewards as $r_t = -\ell_t$, which is equivalent to negating the reward used in the original BYOL-Explore formulation, and can be interpreted as negating the exploration objective to ensure that the agent stays close to the trajectory distribution found in the original dataset.

A.2 Video Model Hyperparameters

Table 1: Hyperparameters and training details for all VQ-GAN models

	DMC	Atari	RLBench (single + multi task)
Input size	$64 \times 64 \times 3$	$64 \times 64 \times 3$	$64 \times 64 \times 3$
Latent size	8×8	16×16	16×16
β (commitment loss coefficient)	0.25	0.25	0.25
Batch size	128	128	128
Learning rate	10^{-4}	10^{-4}	10^{-4}
Learning rate schedule	constant	constant	constant
Training steps	200k	200k	200k
Base channels	128	128	128
Ch mult	[1, 1, 2, 2]	[1, 2, 2]	[1, 2, 2]
Num res blocks	1	1	2
Codebook size	1024	1024	1024
Codebook dimension	64	64	64
Perceptual loss weight	0.1	0.1	0.1
Disc base features	32	32	32
Disc gradient penalty weight	10^8	10^8	10^8
Disc max hidden feature size	512	512	512
Disc mbstd group size	4	4	4
Disc mbstd num features	1	1	1
Disc loss weight	0.1	0.1	0.1

Table 2: Hyperparameters and training details for all VideoGPT and MaskGit models

	DMC	Atari	RLBench (single task)	RLBench (multi-task)
Sequence length	16	16	4	4
Frame skip	1	1	4	4
Latent size	8×8	16×16	16×16	16×16
Number of classes	16	8	n/a	34
Batch size	32	32	32	32
Learning rate	10^{-4}	10^{-4}	10^{-4}	10^{-4}
Learning rate schedule	constant	constant	constant	constant
Training steps	500k	500k	500k	500k
Adam (β_1, β_2)	(0.9, 0.999)	(0.9, 0.999)	(0.9, 0.999)	(0.9, 0.999)
Hidden dim	256	512	256	512
Feedforward dim	1024	2048	1024	2048
Number of heads	8	8	8	8
Number of layers	8	8	8	8
Dropout	0	0	0	0

A.3 Reinforcement Learning Hyperparameters

Table 3: Hyperparameters and training details for DreamerV3

	DMC	Atari	RLBench (single task)	RLBench (multi-task)
General				
Replay Capacity (FIFO)	10^6	10^6	10^6	10^6
Start learning (prefill)	0	0	0	0
Batch Size	16	16	16	16
Batch length	64	64	64	64
MLP Size	2×512	4×1024	4×1024	4×1024
Activation	LayerNorm + swish			
World Model				
RSSM Size	512	4096	4096	4096
Number of Latents	32	32	32	32
Classes per Latent	32	32	32	32
KL Balancing	0.667	0.667	0.667	0.667
Actor Critic				
Imagination Horizon	15	15	15	15
Discount	0.995	0.995	0.995	0.995
Return Lambda	0.95	0.95	0.95	0.95
Target Update Interval	50	50	50	50
All Optimizers				
Gradient Clipping	100	100	100	100
Learning Rate	10^{-4}	10^{-4}	10^{-4}	10^{-4}
Adam epsilon	10^{-6}	10^{-6}	10^{-6}	10^{-6}
Plan2Explore				
Ensemble size	10	10	10	10

Table 4: Hyperparameters and training details for DrQ

	DMC
Actor Critic	
MLP Size	256×256
CNN Features	$32 \times 64 \times 128 \times 256$
CNN Filters	$3 \times 3 \times 3 \times 3$
CNN Strides	$2 \times 2 \times 2 \times 2$
Learning Rate	$3e - 4$
Discount	0.99
Number of Critics	2
τ	0.005
Init Temperature	0.1
Augmentations	Random crop
Random Network Distillation	
RND CNN Features	$32 \times 64 \times 64$
RND MLP Size	512×512
RND learning rate	$3e - 4$
RND Exploration Weight	1

A.4   Environment Training Curves
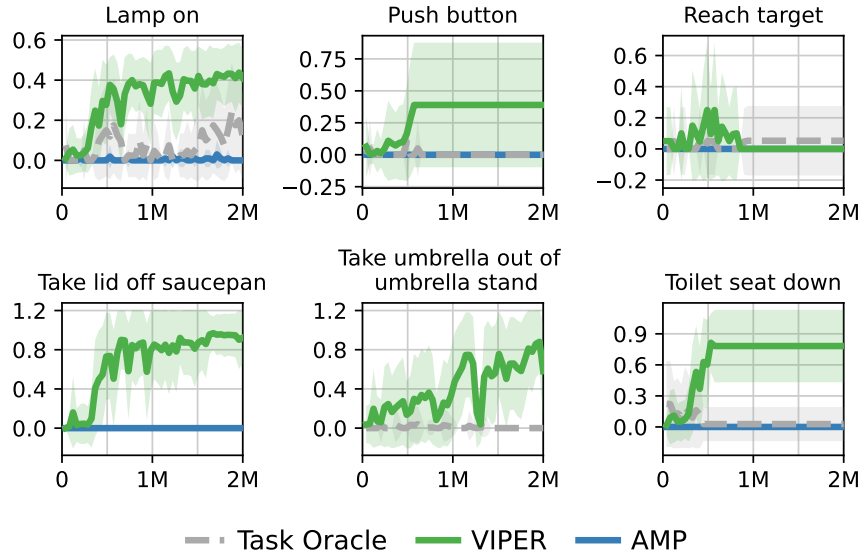
Figure 10: Results across 6 Reinforcement Learning Benchmark tasks, with mean and standard deviation computed across 3 seeds.
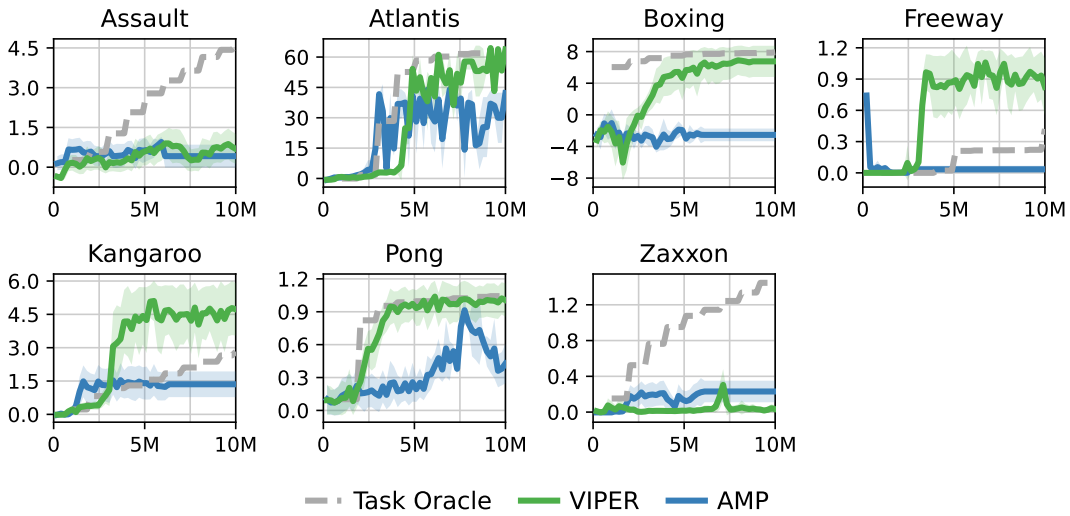
Figure 11: Results across 7 Atari tasks. Scores computed using Human-Normalized Mean across 3 seeds.

17
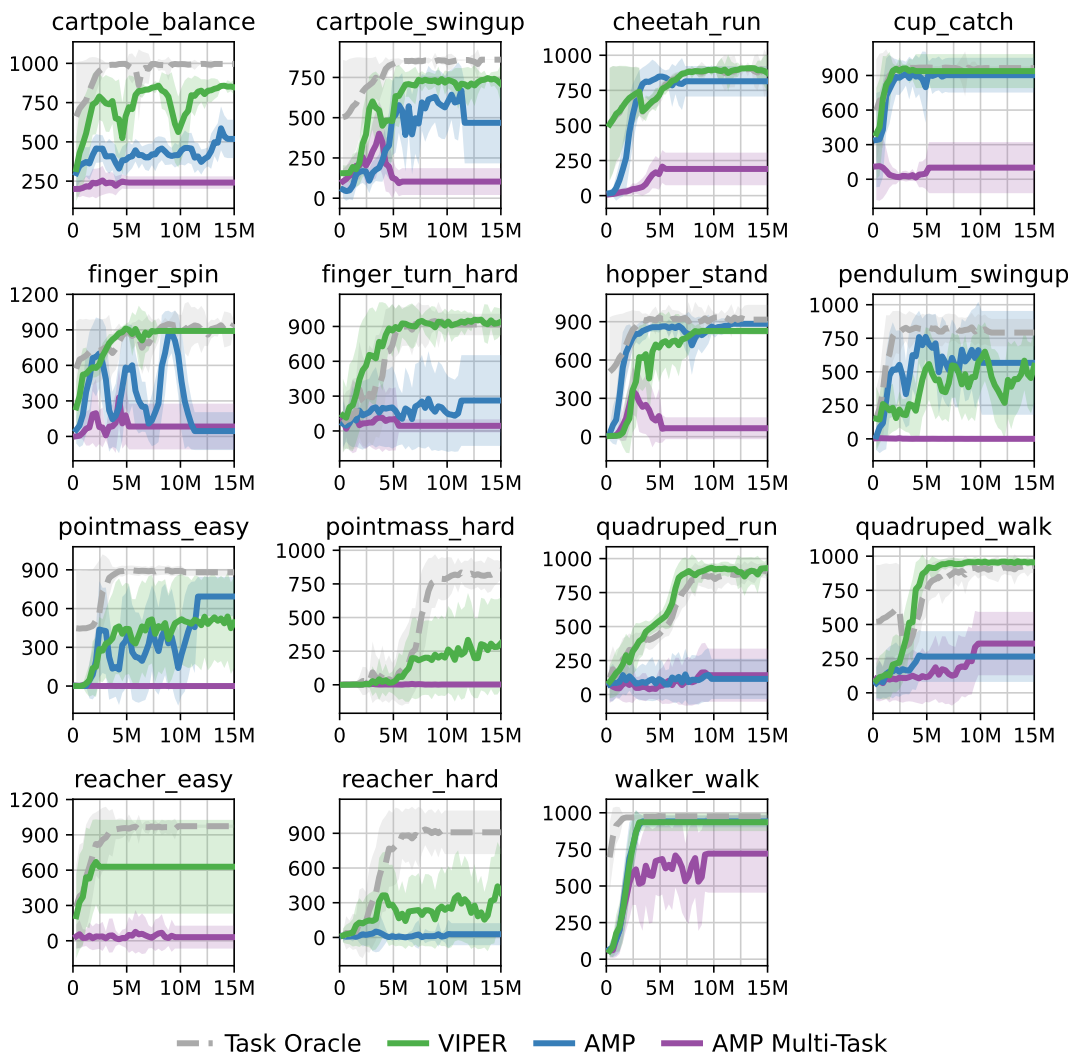
Figure 12: Results across 15 DeepMind Control Suite tasks, with mean and standard deviation computed across 3 seeds. AMP runs were stopped early due to poor performance.

A.5 Training Environments

Figure 13: A single autoregressive video model is trained on 30 tasks for the Franka Panda and 23 tasks for the ReThink Robotics Sawyer, using 16×16 VQCodes and a context length of 4, with frame skip 4.
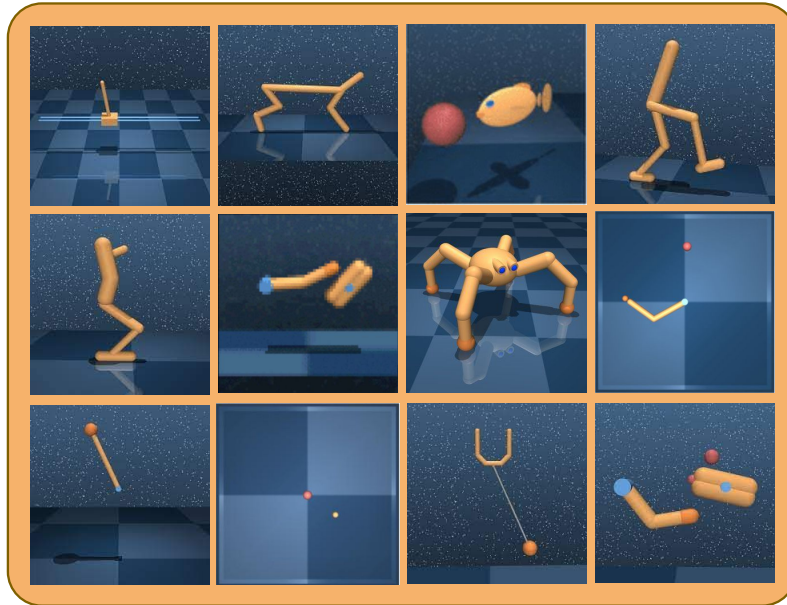
Figure 14: A single task-conditioned autoregressive video model is trained on 15 DeepMind Control Tasks, using 8×8 VQCodes and a context length of 16.

Figure 15: A single autoregressive video model is trained on 7 Atari tasks, using 16×16 VQCodes and a context length of 16.

A.6 Visualizing Video Prediction Uncertainty

Video model uncertainty can be visualized by upsampling the conditional likelihoods over VQCodes. Since VQCodes tend to model local features, this provides a useful tool for analyzing which regions of the image the video model is uncertain about. We visualize video prediction uncertainty for three environments below:
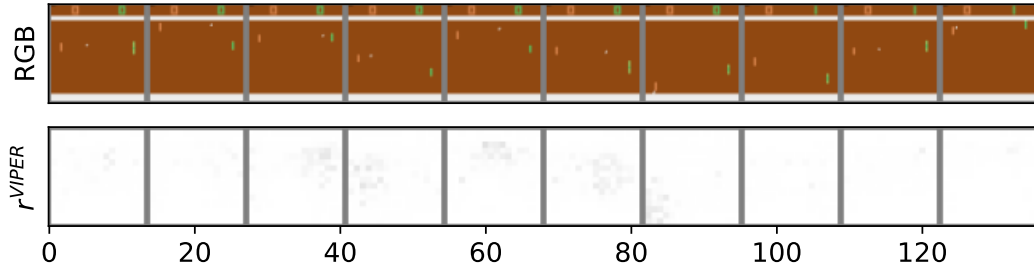
(a) Reference Trajectory
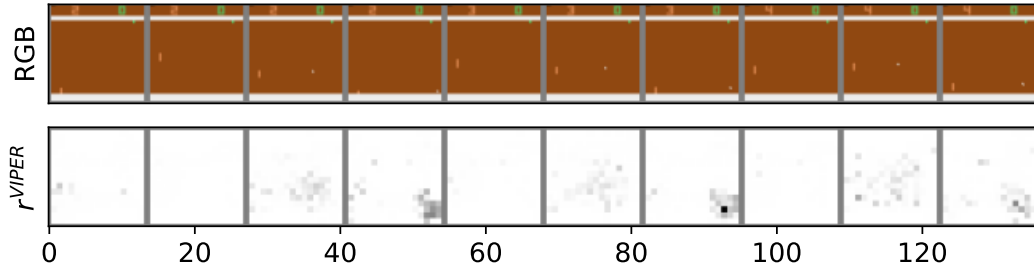
(b) Random Trajectory

Figure 16: Uncertainty visualized for a reference trajectory (top) and a random trajectory (bottom). Brighter values correspond to higher likelihoods. For the random trajectory, the video model assigns lower likelihoods to regions of the image containing the ball. This is especially true for random trajectories, where the video model, trained solely on expert trajectories, cannot accurately predict what happens when the agent plays sub-optimally.
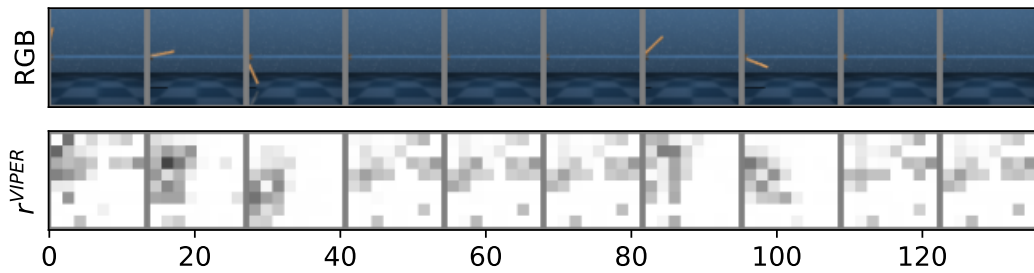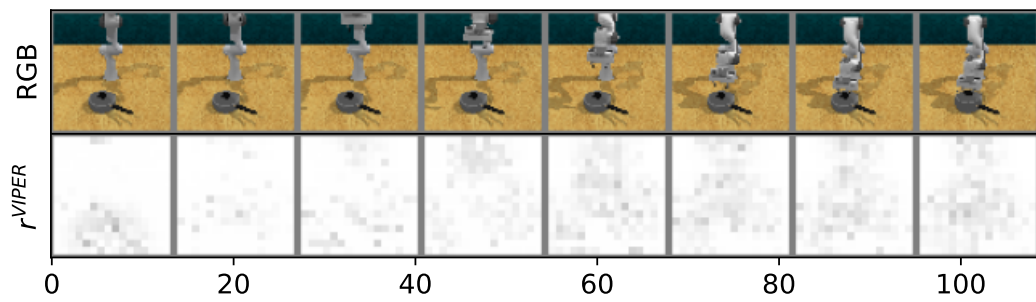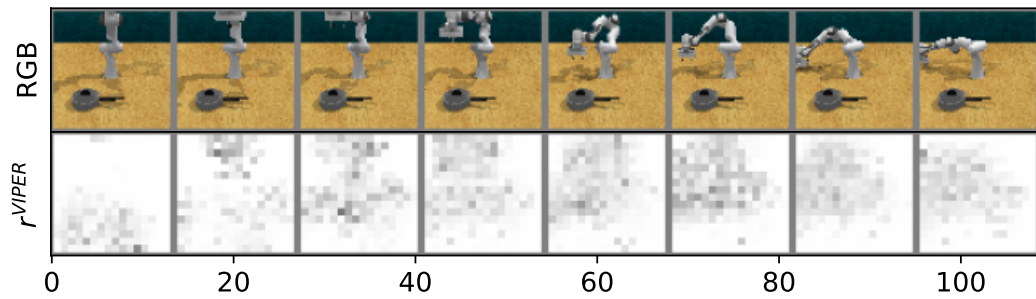

Figure 17: Uncertainty visualized for a random trajectory from the dmc cartpole balance task. Brighter values correspond to higher likelihoods.

(a) Reference Trajectory

(b) Random Trajectory

Figure 18: Uncertainty visualized for a reference trajectory (top) and a random trajectory (bottom). Brighter values correspond to higher likelihoods. Notice the high uncertainty over the position of objects on the table for the first frame. This corresponds to the unconditional likelihood (with no context). Since the position of the saucepan is randomized for every episode, the video model assigns some uncertainty to this initial configuration. For the random trajectory, there is high uncertainty assigned to the position of the arm since the video model has not seen trajectories that display poor behavior.